

Electronic Supplementary Information (ESI) for
Stability limits of elemental 2D metals in graphene pores

Janne Nevalaita and Pekka Koskinen

Department of Physics, Nanoscience Center, University of Jyväskylä, 40014 Jyväskylä, Finland

Email: pekka.koskinen@iki.fi

1 Equivalence of surface and edge energies

In this section we rationalize the relation between edge and surface energies, $\sigma \approx \lambda/d_{2D}$. The relation would be acceptable simply by remarking that the edge of a monolayer has thickness d_{2D} and thus costs σd_{2D} per unit length, but this remark contains subtle caveats that can be avoided by the following derivation.

Let $E_s(a, b, c)$ be the energy of a rectangular slab with sides a, b and height c . Cutting the slab in half trough route (1) (Fig. S1a) gives

$$E_s(a, b, c) = 2\sigma bc + 2E_s(a/2, b, c), \quad (1)$$

where σ is the surface energy. Consider then the successive peeling, cutting, and reassembling of our slab trough another route (2) (Fig. S1a). Following this second route gives

$$E_s(a, b, c) = E_p(a, b, c) + N_L 2\lambda b - 2E_p(a/2, b, c) + 2E_s(a/2, b, c), \quad (2)$$

where λ is the edge energy and E_p is the energy required to peel the slab into N_L monolayers. For large slabs $E_p(a, b, c) \approx 2E_p(a/2, b, c)$ and for close packed structures $N_L \approx c/d_{2D}$, where d_{2D} is the 2D bond length. Therefore, combining equations (1) and (2) and assuming isotropy gives the relation $\sigma \approx \lambda/d_{2D}$, which holds reasonably well for all metals (Fig. S1b).

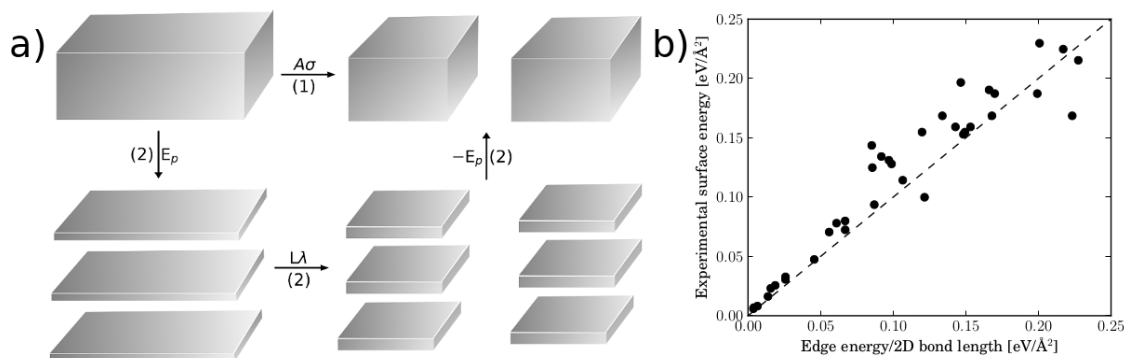


Figure S1 a) Sketch of the scheme to connect edge and surface energies. b) Experimental surface energy as a function of edge energy divided by the 2D bond length for 36 metals. The edge energies were adopted from Ref. 1.

2 Computational methods

We used density functional theory (DFT) as implemented in the GPAW-code^{2,3} with Perdew, Burke, and Ernzerhof (PBE) exchange and correlation (XC) functional⁴ in all calculations. While PBE functional is not the most accurate XC approximation, it is non-empirical, has been used for multiple different types of systems and thus enables broad comparison of our calculations, and is known to reproduce trends, which anyhow represent the focus of our simulations. While van der Waals interactions are important for adsorption on top of graphene, the general trends we establish have sufficient accuracy without resorting to a non-local van der Waals XC functional.

The adsorption, interface, and carbide formation energies were calculated in the plane-wave mode using computational parameters similar to our previous work⁵. The cutoff energy was 800 eV and all calculations were spin polarized. The zigzag-ribbon systems for atom adsorption (Fig. S2b) used $1 \times 4 \times 1$ Monkhorst-Pack k -point sampling^{6,7} while rest of the ribbon systems (Fig. S2a,c,d) used $1 \times 12 \times 1$ sampling. The carbide systems had $12 \times 12 \times 1$ sampling. A vacuum of 5 Å separated atoms from the non-periodic unit cell edges. The Cu clusters on nanoporous graphene were calculated using GPAW's LCAO mode with dzp basis⁸. The k -space was sampled in the Γ -point and all calculations were spin compensated.

The molecular dynamics simulation used a 2 fs time step and a Langevin thermostat set to 300 K with a friction parameter of 0.01. Simulation started from a relaxed structure and was followed by a 2 ps warm-up to 300 K.

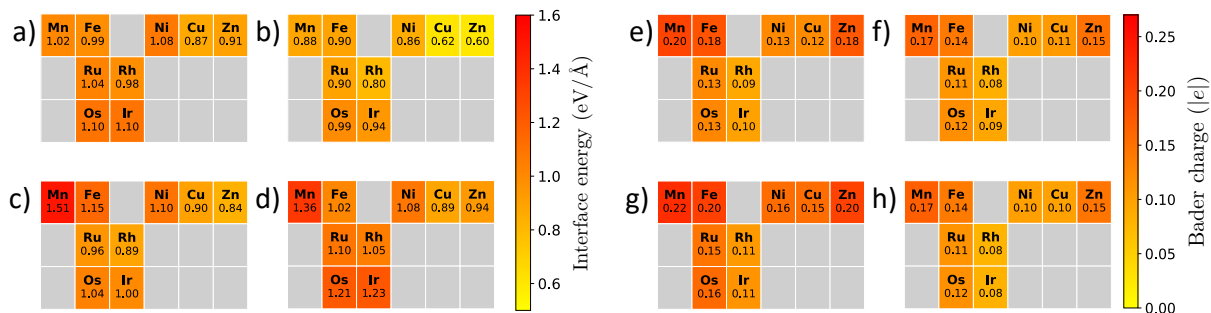


Figure S4 Metal-graphene interface energies for different configurations (Figs. S2c and S2d): a) armchair hollow, b) armchair bridge, c) zigzag hollow, and d) zigzag top sites. Bader charger per metal atom for different metal-graphene interface configurations (Figs. S2c and S2d): e) armchair hollow, f) armchair bridge, g) zigzag hollow, and h) zigzag top sites.

5 Metal carbides

Motivated by previous global optimization studies¹⁰, metal carbides were considered in three geometries: M_1C_1 (Fig. S5a), M_2C_1 (Fig. S5b), and another, C-dimer variant of M_1C_1 (Fig. S5c). The geometries and unit cells were optimized to maximum force of 0.005 eV/Å^{11,12}. The geometries shown in Fig. S5 are representative; for some metals the unit cells were distorted.

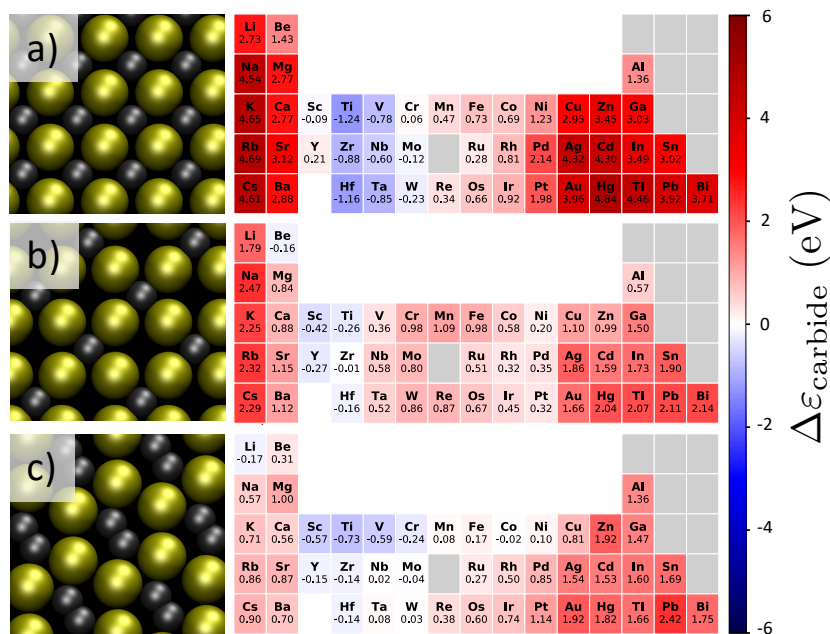


Figure S5 Carbide formation energies as defined in Eq. (7) for three different geometries shown in the left hand panels: a) M_1C_1 , b) M_2C_1 , and c) another M_1C_1 geometry. Negative (blue) value means an exothermic carbide formation process.

6 Summative figure of merit of 2D patch stability

The purpose of the figure of merit is to consider several competing viewpoints simultaneously in order to rank the metals to identify the most stable 2D patches. The merit considered the following viewpoints:

1. Intrinsic relative stability of the 2D metal, including two viewpoints:
 - i) the Δ -parameters from Eq. (6) (Fig. 2c; smaller is better) and
 - ii) the bending moduli from Fig. 10 of Ref.⁵ averaged over square and hexagonal lattices (larger is better).
2. Commensurability and the resulting strain energy at the interface (Fig. S6; smaller is better).
3. Unfavorable formation of carbides (Fig. 3b; larger is better)
4. Chemical binding strength at the interface (Fig. 3a; larger is better).

The figure of merit was then calculated as the root-mean-square ranking across all the viewpoints. We experimented with different schemes of constructing the figure of merit, but Cu was invariably the best candidate; the ranking of other prominent

metals varied, though not excessively. We calculated also template-independent figure of merit using only the intrinsic 2D stability (Δ -parameter) and bending moduli. In this generic case the best candidates are Au, Be, Pt, and Cu (Fig. S7).

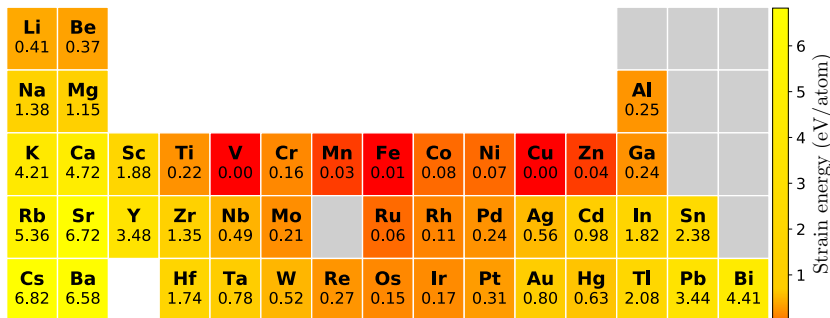


Figure S6 Strain energy in metals due to lattice mismatch with respect to graphene. The energy is calculated as $E_s = \sqrt{3} B d_{2D}^2 \epsilon^2$, where B is the 2D bulk modulus (numbers taken from Table I of Ref.⁵) and ϵ is the lattice strain with respect to graphene (Fig. 3c).

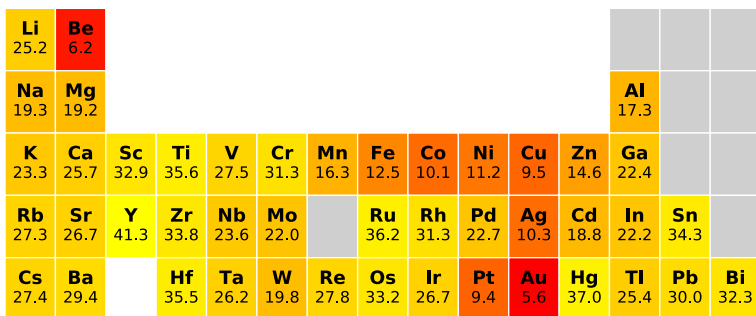


Figure S7 Template-independent figure of merit, accounting only intrinsic 2D stability and the magnitudes of bending moduli.

7 DFT calculations of finite Cu patches

The graphene nanopores were made either spherical or hexagonal, depending on the number of Cu atoms. Two C atoms were removed for each added Cu atom. The 3D clusters were optimized starting from the cluster structures given by the Lennard-Jones potential. For consistency, the pore structures for given N were the same in all three cases. Fig. S8 shows 10 examples of the optimized structures.

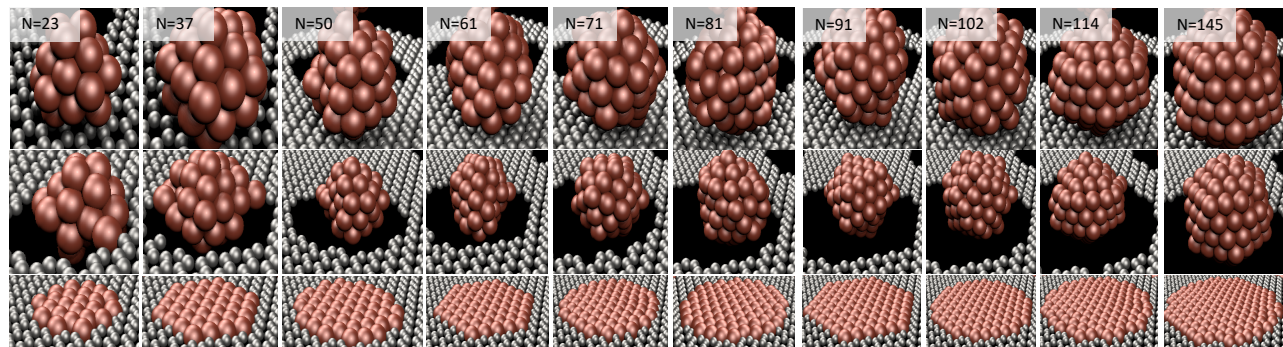


Figure S8 Examples of optimized Cu clusters in graphene pores. The top panels show on-top-adsorbed 3D clusters, middle panels pore edge-adsorbed 3D clusters, and bottom panels 2D patches inside pores.

Notes and references

- [1] J. Nevalaita and P. Koskinen, *Phys. Rev. B*, 2018, **98**, 115433.
- [2] J. J. Mortensen, L. B. Hansen and K. W. Jacobsen, *Phys. Rev. B*, 2005, **71**, 035109.
- [3] J. Enkovaara, C. Rostgaard, J. J. Mortensen, J. Chen, M. Duřak, L. Ferrighi, J. Gavnholt, C. Glinsvad, V. Haikola, H. A. Hansen, H. H. Kristoffersen, M. Kuisma, A. H. Larsen, L. Lehtovaara, M. Ljungberg, O. Lopez-Acevedo, P. G. Moses,

J. Ojanen, T. Olsen, V. Petzold, N. A. Romero, J. Stausholm-Møller, M. Strange, G. A. Tritsarlis, M. Vanin, M. Walter, B. Hammer, H. Häkkinen, G. K. H. Madsen, R. M. Nieminen, J. K. Nørskov, M. Puska, T. T. Rantala, J. Schiøtz, K. S. Thygesen and K. W. Jacobsen, *J. Phys. Condens. Matter*, 2010, **22**, 253202.

- [4] J. P. Perdew, K. Burke and M. Ernzerhof, *Phys. Rev. Lett.*, 1996, **77**, 3865–3868.
- [5] J. Nevalaita and P. Koskinen, *Phys. Rev. B*, 2018, **97**, 035411.
- [6] H. J. Monkhorst and J. D. Pack, *Phys. Rev. B*, 1976, **13**, 5188–5192.
- [7] J. D. Pack and H. J. Monkhorst, *Phys. Rev. B*, 1977, **16**, 1748–1749.
- [8] A. H. Larsen, M. Vanin, J. J. Mortensen, K. S. Thygesen and K. W. Jacobsen, *Phys. Rev. B*, 2009, **80**, 195112.
- [9] I. A. Pašti, A. Jovanović, A. S. Dobrota, S. V. Mentus, B. Johansson and N. V. Skorodumova, *Appl. Surf. Sci.*, 2018, **436**, 433–440.
- [10] Y. Shao, R. Pang and X. Shi, *J. Phys. Chem. C*, 2015, **119**, 22954–22960.
- [11] E. B. Tadmor, G. S. Smith, N. Bernstein and E. Kaxiras, *Phys. Rev. B Condens. Matter Mater. Phys.*, 1999, **59**, 235–245.
- [12] E. Bitzek, P. Koskinen, F. Gähler, M. Moseler and P. Gumbsch, *Phys. Rev. Lett.*, 2006, **97**, 170201.